THE JOURNAL OF PHYSICAL CHEMISTRY C

Article

Cite This: J. Phys. Chem. C 2018, 122, 9480−9490

pubs.acs.org/JPCC

Bilayer Formation vs Molecular Exchange in Organic Heterostructures: Strong Impact of Subtle Changes in Molecular Structure

Qi Wang,[†,‡,⊥] Antoni Franco-Cañellas,[‡,⊥] Penghui Ji,[†] Christoph Bürker,[‡] Rong-Bin Wang,[†,§] Katharina Broch,[‡] Pardeep Kumar Thakur,[∥] Tien-Lin Lee,[∥] Haiming Zhang,[†] Alexander Gerlach,[‡] Lifeng Chi,*[,†] Steffen Duhm,*[,†] and Frank Schreiber*[,‡]

[†]Institute of Functional Nano & Soft Materials (FUNSOM), Jiangsu Key Laboratory for Carbon-Based Functional Materials & Devices and Joint International Research Laboratory of Carbon-Based Functional Materials and Devices, Soochow University, 215123 Suzhou, People's Republic of China

[‡]Institut für Angewandte Physik, Universität Tübingen, 72076 Tübingen, Germany

[§]Institut für Physik & IRIS Adlershof, Humboldt-Universität zu Berlin, 12489 Berlin, Germany

[∥]Diamond Light Source, Harwell Science and Innovation Campus, OX11 0DE Oxfordshire, United Kingdom

Supporting Information

ABSTRACT: Organic heterostructures are a central part of a manifold of (opto)electronic devices and serve a variety of functions. Particularly, molecular monolayers on metal electrodes are of paramount importance for device performance as they allow tuning energy levels in a versatile way. However, this can be hampered by molecular exchange, i.e., by interlayer diffusion of molecules toward the metal surface. We show that the organic−metal interaction strength is the decisive factor for the arrangement in bilayers, which is the most fundamental version of organic−organic heterostructures. The subtle differences in molecular structure of 6,13-pentacenequinone (P2O) and 5,7,12,14-pentacenetetrone (P4O) lead to antithetic adsorption behavior on Ag(111): physisorption of P2O but chemisorption of P4O. This allows providing general indicators for organic−metal coupling based on shifts in photoelectron spectroscopy data and to show that the coupling strength of copper-phthalocyanine (CuPc) with Ag(111) is in between that of P2O and P4O. We find that, indeed, CuPc forms a bilayer when deposited on a monolayer P4O/Ag(111) but molecular exchange takes place with P2O, as shown by a combination of scanning tunneling microscopy and X-ray standing wave experiments.

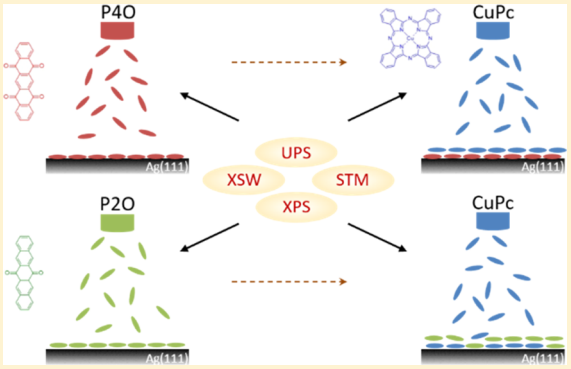

INTRODUCTION

The energy-level alignment between active conjugated organic materials (COMs) and metal electrodes is of paramount importance for charge transport across the metal−organic interface and thus an eminent factor for the efficiency of organic (opto)electronic devices.[1,2] Template layers between the metal contact and the active material have been proven an efficient way for engineering interface energetics and tuning energy barriers for charge injection/withdrawal.[3,4] However, molecular diffusion can be a serious issue in the actual arrangement within the bilayer that does not necessarily reflect the deposition sequence.[5−7] In particular, for weak coupling at an organic−metal interface, subsequently deposited COMs can diffuse through the template layer to the metal surface,[5,8−11] making the template layer obsolete. Whether such molecular exchange takes place is, moreover, a fundamental question by itself, which has been addressed in bilayer model system studies.[9−18]

Although there are several studies about organic heterostructures on clean metal surfaces focusing on bimolecular monolayers,[19−23] only few studies focus on bilayers[9−18,24,25] and bilayers of copper-phthalocyanine (CuPc) and 3,4,9,10-perylene-tetracarboxylic-dianhydride (PTCDA) on Ag(111) evolved as a model system.[11,14,15,24,25] For PTCDA deposition on a closed layer of CuPc on Ag(111), molecular exchange takes place and PTCDA reaches the Ag(111) surface,[11] whereas for the inverse system, i.e., CuPc on PTCDA, the initial bilayer arrangement is maintained.[14,15] As expected, the coupling of CuPc with Ag(111) is relatively weak,[26,27] whereas PTCDA is comparatively strongly coupled to the same substrate.[28−31] Going beyond this model system, we show in the present work that the organic−metal interaction strength is indeed a decisive

Received: February 12, 2018
Revised: April 3, 2018
Published: April 18, 2018

DOI: 10.1021/acs.jpcc.8b01529
J. Phys. Chem. C 2018, 122, 9480−9490

factor for the sequential arrangement in organic heterostructures.

Interfacial "interaction strength" is well-defined and comparable from a theoretical viewpoint.[32−35] However, computing reliable adsorption energies of COMs on surfaces involves an advanced level of theory and, moreover, still requires experimental input, e.g., surface unit cells.[34,36] Therefore, we attempt to develop experimentally accessible indicators for the organic−metal interaction strength based on:

(1) vacuum-level (VL) shifts (ΔVL),
(2) binding-energy (BE) shifts of:
   i. valence electron features (ΔHOMO),
   ii. core levels of aromatic carbon atoms (ΔC_{π}),
   iii. core levels of carbon atoms in functional groups (ΔC_{funct}),
(3) averaged vertical bonding distances (d_H).

Indicators #1 and #2 are based on widely used photoelectron spectroscopy and indicator #3 can be accessed with the X-ray standing wave (XSW) technique.[37,38] Although it is hard to prove the absolute generality of these indicators, our work shows that most of these indicators are consistent for the cases considered.

The organic−metal interaction strength is the result of various competing effects, such as van der Waals interactions, charge transfer, or Pauli push back, and a broad range of scenarios was reported in a number of detailed studies over the last decades.[19,33,34,39−43] As a striking example, for the subtle competition of interactions, 6,13-pentacenequinone (P2O) and 5,7,12,14-pentacenetetrone (P4O) (chemical structures in Figure 1) have been studied.[44] Both COMs are physisorbed

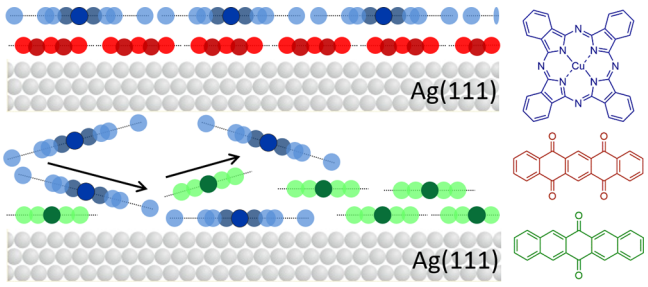

Figure 1. Bilayer formation (top) vs molecular exchange (bottom). In both cases, CuPc (blue) has been vacuum-sublimed on a closed monolayer of P4O (red) or P2O (green) on Ag(111). On the right side, the chemical structures of CuPc, P4O, and P2O are shown.

on Au(111) with a planar adsorption geometry and large bonding distances. In contrast, on Cu(111) they are chemisorbed involving a net electron transfer from the substrate to the adsorbate, resulting in a (partially) filled former lowest unoccupied molecular orbital (LUMO). The monolayer core levels show strong chemical shifts, and the molecules adsorb in a bent conformation with short bonding distances. Ag(111) as a substrate provides an intermediate case, and by simply adding two more oxygen atoms to the molecular structure, the interaction can be changed from physisorption (P2O) to chemisorption (P4O).[44]

For our model study, we use PxO (x = 2, 4) to modify Ag(111). As shown by our ultraviolet photoelectron spectroscopy (UPS) data, the vacuum level of Ag(111) decreases by adsorption of a monolayer of P2O (mainly by push back) but stays virtually constant for a monolayer of P4O (push back compensated by charge transfer). The vacuum level shift induced by a monolayer of CuPc on Ag(111) is just in between the ΔVLs of the two pentacene derivatives on the same substrate. Assuming bilayer formation and vacuum-level alignment at the organic−organic interface, precovering Ag(111) by PxO should thus either lower the hole- or the electron-injection barrier into subsequently deposited CuPc. Importantly, by means of scanning tunneling microscopy (STM) we show that bilayer formation takes place only for P4O as a template layer. By XSW measurements, it becomes apparent that bilayer formation has only a small impact on vertical organic−metal bonding distances. X-ray photoelectron spectroscopy (XPS) data reveal the chemical interaction of the three COMs with Ag(111). Overall, we provide a comprehensive picture of lateral as well as vertical order, chemical interaction at the inorganic/organic and organic/organic interfaces, and interface energetics.

METHODS

UPS, XPS, and low-energy electron diffraction (LEED) experiments were carried out in an ultrahigh vacuum system[45] consisting of three interconnected chambers: evaporation chamber (base pressure: 3×10^{-10} mbar), annealing and sputtering chamber (3×10^{-10} mbar), and analysis chamber (base pressure: 2×10^{-10} mbar). The Ag(111) substrate was cleaned by several cycles of Ar^+ ion bombardment and annealing (650−700 K). The COMs have been sublimated onto the single-crystal surface (held at room temperature) by physical vapor deposition from home-built, resistively heated Knudsen cells with deposition rates of about 1−2 Å/min. The nominal film mass thickness was monitored with a quartz-crystal microbalance positioned near the samples within the deposition chamber. UPS experiments were performed using monochromatized He I radiation (21.2 eV) and a Specs PHOIBOS 150 analyzer. The energy resolution was set to 80 meV. The angle between the incident beam and the sample was fixed to 40°. The spectra were collected at photoelectron take-off angles (θ) of 45° with an acceptance angle of ±10° along the Γ−M direction of Ag(111). A sketch of the measurement geometry can be found in ref 46. The secondary electron cut-off (for determination of the vacuum level) was measured in normal emission with a bias potential of −3 V. XPS was performed using a monochromatized Al Kα source (1486.6 eV). The data analysis was carried out by a nonlinear least-square fitting routine, using Gaussian/Lorentzian peak shapes and a Shirley background. The error of BE values in UPS is estimated to be ±0.05 eV. LEED experiments were performed using a Micro-Channel-Plate LEED (OCI BDL800IR-MCP).

The normal-incidence XSW experiments were performed at the beamline I09[47] of Diamond Light Source (DLS), Didcot, U.K. The analysis chamber (base pressure, 3×10^{-10} mbar) contains a VG Scienta EW4000 HAXPES hemispherical electron analyzer, which is mounted at ∼90° relative to the incident X-ray beam. Sample preparation and measurements took place in situ under ultrahigh vacuum conditions. A typical nominal deposition rate was ∼0.2 Å/min. The reflectivity and an XP spectrum of the core level of interest were recorded simultaneously at different photon energies (31 data points) within a ±3 eV interval around the Bragg energy (∼2.63 keV) of the silver (111) diffraction planes. Considering the experimental geometry, the photoelectron yield and the reflectivity were modeled within the dipole approximation.

DOI: 10.1021/acs.jpcc.8b01529
J. Phys. Chem. C 2018, 122, 9480−9490

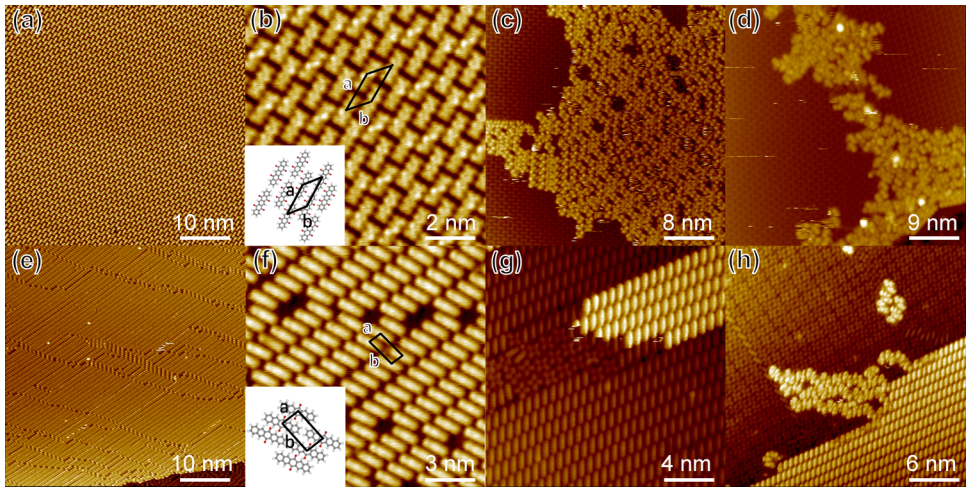

Figure 2. Each row displays STM images of self-assembled monolayers of P4O (a, b) or P2O (e, f) on Ag(111) and subsequently deposited CuPc on P4O/Ag(111) (c, d) or P2O/Ag(111) (g, h). The insets in (b) and (f) show the proposed unit cells of P4O/Ag(111) (a = 1.70 nm, b = 1.12 nm, φ = 40°) and P2O/Ag(111) (a = 0.81 nm, b = 1.59 nm, φ = 86°). All images have been measured with a tunneling voltage of −1 V and a tunneling current of 10 pA (a−d, f, h) or 100 pA (e, g).

All UPS, XPS, LEED, and XSW measurements were performed at room temperature (295 K).

The STM measurements were performed using a commercial low-temperature STM (LT-STM, Omicron NanoTechnology) that contains two chambers: the preparation chamber (P-chamber) with a base pressure of 2×10^{-10} mbar and the STM chamber (2×10^{-11} mbar). The Ag(111) single crystal was cleaned by cycles of Ar^+ sputtering and a high temperature annealing (740 K). A commercial three-cell evaporator (Kentax GmbH, Germany) was used to sublime P2O, P4O, and CuPc at 413, 423, and 600 K, respectively. All samples were prepared in the P-chamber and characterized by STM immediately after deposition. All the STM images were obtained at liquid nitrogen environment (77 K) with a home-built tungsten tip.

RESULTS

All experiments on the heterostructures have in common that first PxO layers on Ag(111) have been prepared by vacuum sublimation. The coverage has been as close to a monolayer as possible. In some cases, multilayers have been desorbed by a careful annealing procedure (Figure S1). In a second step, CuPc has been (stepwise) deposited on the PxO monolayers. All preparation steps as well as XPS, UPS, and XSW measurements have been performed at room temperature. STM data were recorded at 77 K. Additional room temperature LEED experiments of PxO monolayers on Ag(111) (Figure S2) show that molecular order prevails at room temperature.

Molecular Rearrangement Determined by Scanning Tunneling Microscopy. We start with the STM results, which unambiguously show the actual arrangement of the heterostructures. As shown in Figure 2a, P4O molecules form well-defined monolayers on Ag(111). A corresponding structural model is depicted in the inset of the magnified STM image (Figure 2b). To investigate the mixed molecular structure of CuPc on P4O precovered Ag(111) surfaces, CuPc has been deposited gradually on the sample. With increasing CuPc coverage, hardly any structural changes of the P4O monolayers are observed (Figure 2c,d). CuPc molecules adsorb predominantly on P4O monolayers and are not able to disturb the underlying P4O structure.

Figure 2e shows the monolayer structure of P2O. The detailed packing structure of P2O can be gathered from a magnified STM image and the corresponding structural model (see Figure 2f and the inset). In striking contrast to the previous heterostructure involving P4O, CuPc deposited on P2O can replace P2O molecules and form a well-ordered structure directly on Ag(111) (Figure 2g) with a similar packing motif as that of the CuPc/Ag(111) monosystem.[48] The replaced P2O molecules adsorb preferentially on top of the remaining P2O monolayer, forming the second layer. To confirm the adsorption sites of the second P2O layer, molecular manipulation by the STM tip is performed to remove some P2O molecules in the second layer. On the basis of the STM image (Figures S3 and S4), we can conclude that the layer underneath is composed of well-ordered P2O. Only for a much higher CuPc coverage, replaced P2O can also adsorb on top of CuPc layer, forming a disordered structure (Figure 2h).

Core-Level Shifts ΔC_π and ΔC_{funct} Determined by X-ray Photoelectron Spectroscopy. Having established the lateral and the sequential arrangement of the heterostructures, we now turn to the molecular core levels (Figure 3). Chemisorbed systems usually exhibit strong core-level shifts between (charged) monolayers and neutral multilayers,[44,45,49−52] and these shifts (ΔC_π and ΔC_{funct}) can act as indicators for the interaction strength.

The multilayer (nominally 48 Å) C 1s spectrum of CuPc on Ag(111) (Figure 3a) resembles those of multilayers on other substrates[53−55] and the gas phase spectrum.[53] The two main peaks are attributed to carbon atoms in the benzene rings (C−C) and the carbon atoms bound to nitrogen in the pyrrole rings (C−N), respectively. The smaller peak (marked with a red star) at higher BE is due to a shake-up satellite.[53] For a nominal coverage of 4 Å, both monolayer (blue areas) and multilayer (blue areas with pattern) contributions can be seen. In general, for flat-lying COMs, a nominal coverage of around 4 Å would correspond to a closed monolayer[56,57] and the occurrence of mono- as multilayer features for this coverage points thus to island growth. The multilayer C−C-derived peak is found at 0.25 eV higher BE than the monolayer peak; this shift corresponds to ΔC_π. On the other hand, ΔC_{funct} amounts to 0.56 eV. Such nonrigid shifts point to a charge-transfer reaction

DOI: 10.1021/acs.jpcc.8b01529
J. Phys. Chem. C 2018, 122, 9480−9490

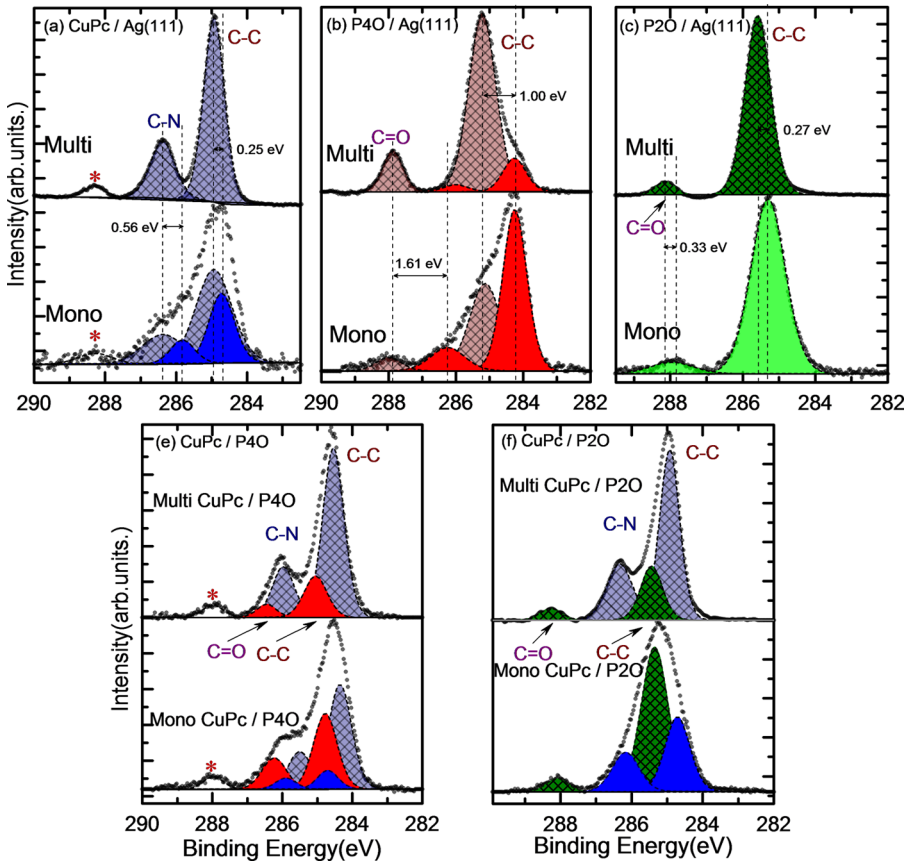

Figure 3. C 1s core-level spectra for homostructures (top row, CuPc in blue, P4O in red, and P2O in green) and heterostructures (bottom row). The nominal coverages are 48 Å (multi) and 4 Å (mono). The fits are color-coded to mark contributions from the different COMs and to distinguish between monolayer (full color) and multilayer (pale color with pattern) contributions. The red star (*) marks a shake-up satellite of CuPc. For the heterostructures, CuPc was deposited on a P*x*O monolayer prepared via annealing a thick film.

of CuPc and Ag(111).[49,50,54] P4O on Ag(111) (Figure 3b) shows a similar phenomenon as that of CuPc. For a nominal coverage of 4 Å, monolayer (red areas) and multilayer (red areas with pattern) contributions are found in the spectra. Here, ΔC_{π} is 1.00 eV and ΔC_{funct} is 1.61 eV, which has been ascribed to a charge transfer by surface-induced aromatic stabilization.[44] The weak interaction of P2O with Ag(111) is reflected in the similar shape and binding-energy position of monolayer and multilayer spectra ($\Delta C_{\pi} \approx \Delta C_{funct} \approx 0.3$ eV) and is fully consistent with previously published data on the same interface.[44]

Taking advantage of real-time XPS during desorption (Figure S1), monolayers of P*x*O could be prepared by thermal desorption of multilayers and have been used as a template for subsequent CuPc deposition. For C 1s, it is hard to disentangle the different contributions of P*x*O and CuPc, respectively (Figure 3e,f). O 1s spectra (Figure 4) give more insight into possible chemical interactions at these interfaces. Depositing nominally 4 Å CuPc on a monolayer P4O/Ag(111) does not lead to significant changes in the shape or the BE position of the O 1s peak. As surface-induced aromatic stabilization of P4O leads to strong chemical shifts between mono- and multilayer (Figure 4 b,c),[44] this further supports the STM finding of bilayer formation. In contrast to P4O, for P2O/Ag(111) multi- and monolayer O 1s spectra are quite similar (Figure 4 e,f) and thus do not allow to judge whether, in the heterostructure, P2O is in direct contact with Ag(111) or pushed away by CuPc. Similarly, the rather weak N 1s signal

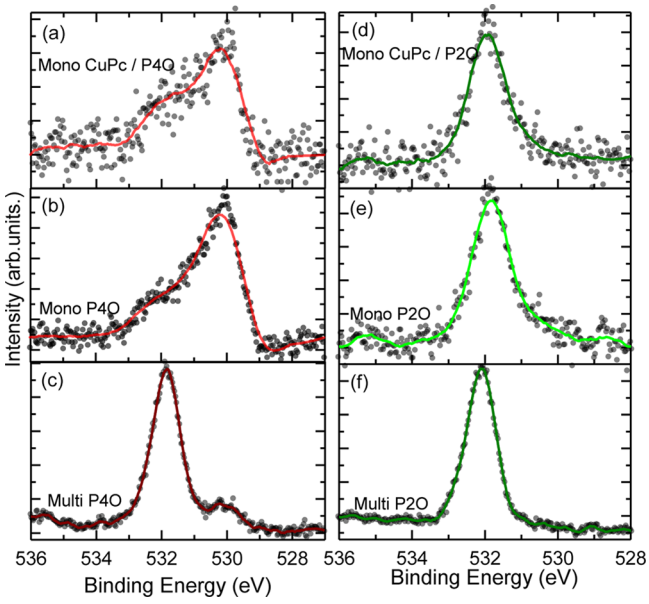

Figure 4. O 1s core-level spectra for mono- and multilayers of P*x*O on Ag(111) and for CuPc monolayer on the respective P*x*O monolayer (by annealing procedure). In each case, the measured data points and a smoothed curve are shown.

(Figure S5) of CuPc does not give further insight in the heterostructure arrangement.

DOI: 10.1021/acs.jpcc.8b01529
J. Phys. Chem. C 2018, 122, 9480−9490

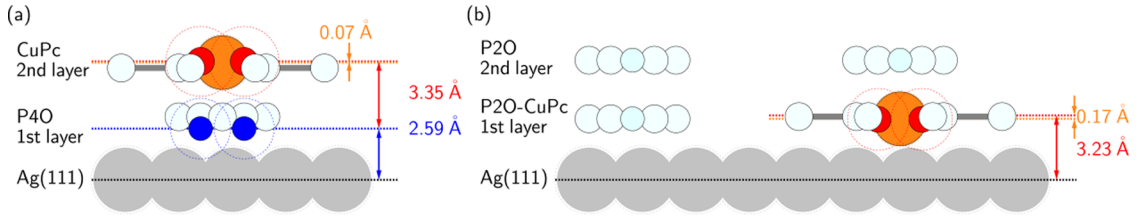

Figure 5. Adsorption distances, as obtained from XSW measurements (Figure S6) of (a) CuPc deposited on a monolayer P4O and (b) the molecular exchange P2O by CuPc. Only the clearly resolved species are highlighted: Cu (orange), nitrogen (red), and the P4O oxygen atoms (blue). The van der Waals radii are shown as dotted lines. Atoms are drawn to scale.

Adsorption Distances d_H Determined by X-ray Standing Wave Measurements. Adsorption distances can be measured very precisely with the XSW technique. The analysis of the photoelectron yield (Figure S6) of an adsorbate measured in the standing wave field generated by the interference of incident and at-the-substrate Bragg-diffracted X-ray waves gives the coherent position (P_H) and coherent fraction (f_H).[58−60] P_H can be used to determine the averaged vertical bonding distance (d_H) of the different adsorbate atoms by $d_H = d_{111}(n + P_H)$, with d_{111} as the lattice spacing of the substrate and n being an integer number, that arises from the periodicity of the standing wave field, which is important when distinguishing between the molecules adsorbing in the first layer and those in the second. f_H is a measure for the degree of vertical order of the respective adsorbate atoms.

For monolayers of PxO on Ag(111), the bonding distances are essentially the same as previously reported.[44] P2O exhibits a planar adsorption geometry with rather long bonding distances. For P4O, the bonding distances are shorter and the oxygen atoms are bent below the plane of the carbon skeleton. The coherent fractions of the carbon and oxygen atoms for P4O are 0.75 and 0.95, respectively, and thus relatively large for these systems. This is due to the strong interfacial coupling, and consequently the coherent fractions for physisorbed P2O are much lower (0.29 and 0.41, respectively). Overall, the coherent fractions of the monolayers prepared by desorbing multilayers (this work) are higher than those for the directly vacuum-sublimed-grown (sub)monolayers.[44] This indicates that the method used here to prepare the monolayers may help to improve the ordering (higher f_H) of the remaining layer. However, as f_H depends on the specific experimental conditions[40,61] and as especially the employed setup tends to overestimate coherent fractions,[62] we refrain from further discussion.

For the heterostructures (Figure 5), coherent positions and fractions could be measured for O, Cu, and N atoms. For C atoms, the photoelectron yield could not be properly evaluated because the contributions of PxO and CuPc to the C 1s signal could not be disentangled. Nonetheless, the deposition of CuPc on a monolayer P4O/Ag(111) leaves the oxygen atoms unaffected, similar to the CuPc/PTCDA case.[15] The N atoms of CuPc are found 3.35 Å and the Cu atoms 3.28 Å above the O atoms of P4O (Figure 5a), similar to those of CuPc on PTCDA.[15] For the deposition of CuPc on P2O/Ag(111), the results are in line with the STM finding of the molecular exchange, since physically meaningful adsorption distances can only be obtained by considering that CuPc is in direct contact with the substrate and P2O occupies positions in the first as well as in the second layer. The N and Cu atoms of CuPc have averaged bonding distance of 3.23 and 3.06 Å, respectively, which is slightly higher than that for CuPc (sub)monolayers on Ag(111).[27] The coherent fractions of the O atoms are rather low (0.24) and do not allow a proper assignment of bonding distances, which is due to P2O molecules being present at different vertical sites (Figure 5b). In this scenario, the measured shorter adsorption distances of CuPc, when coexisting with P2O in the first layer, are in line with other investigated heteromolecular monolayers, where a change in adsorption distances takes place.[11,63−65] In particular, the molecules with the strongest donor character move closer to the substrate and those with an acceptor (or weaker donor) behavior move away from it.[63−65] Therefore, we expect P2O to have a reduced adsorption distance compared with the monomolecular film, possibly involving the slight bending of the oxygen atoms relative to the carbon core.

Valence-Level Shifts ΔHOMO Determined by Ultraviolet Photoelectron Spectroscopy. The coverage-dependent evolution of valence-electron spectra of the homostructures (Figure 6) confirms previous results.[27,44,52,66] Deposition of CuPc on Ag(111) (Figure 6a) attenuates the intensity of the substrate-derived Fermi edge, and two CuPc-derived peaks arise: the highest occupied molecular orbital (HOMO)-derived peak centered at 1.37 eV (for a nominal coverage of 4 Å) and a peak close to E_F, derived from the former, now partially filled, LUMO (F-LUMO).[27] The intensity of this peak becomes strongest at nominal monolayer coverage (4 Å), and increasing the coverage leads to an attenuation of this feature as the charge transfer does not extend beyond the monolayer. For multilayer coverage, the HOMO peak shifts to higher BE (ΔHOMO = 0.35 eV) and, moreover, its shape is distinctively different to that in the monolayer, which is due to molecular relaxation upon charge transfer and is in good agreement with a previous, very detailed, study.[27] Likewise, also for P4O on Ag(111) (Figure 6b), spectral features assigned to HOMO and F-LUMO[44] can be observed for monolayer coverage. The shift of the HOMO position between mono- and multilayer coverage amounts to ΔHOMO = 0.95 eV. For physisorbed P2O on Ag(111) (Figure 6c), almost no F-LUMO-derived photoemission intensity can be observed and the shift of the HOMO (ΔHOMO = 0.50 eV) can be mainly ascribed to the screening effect.[44] A closer look reveals a small photoemission intensity close to E_F, which becomes more prominent for the annealed monolayer (Figures 6e and S7). As detailed in the Discussion, this observation is most likely due to Fermi-level pinning[67,68] of the P2O LUMO and thus not conflicting with the physisorption scenario, which has been suggested in ref 44.

Figure 6d,e shows the spectra of CuPc (blue lines) deposited on PxO-precovered Ag(111) (red and green lines). The shape and the position of the HOMO-derived peak of CuPc deposited on P4O Ag(111) do not show a notable coverage-dependent change and are reminiscent of the CuPc multilayer. This is in line with CuPc and P4O forming a bilayer system on

DOI: 10.1021/acs.jpcc.8b01529
J. Phys. Chem. C 2018, 122, 9480−9490

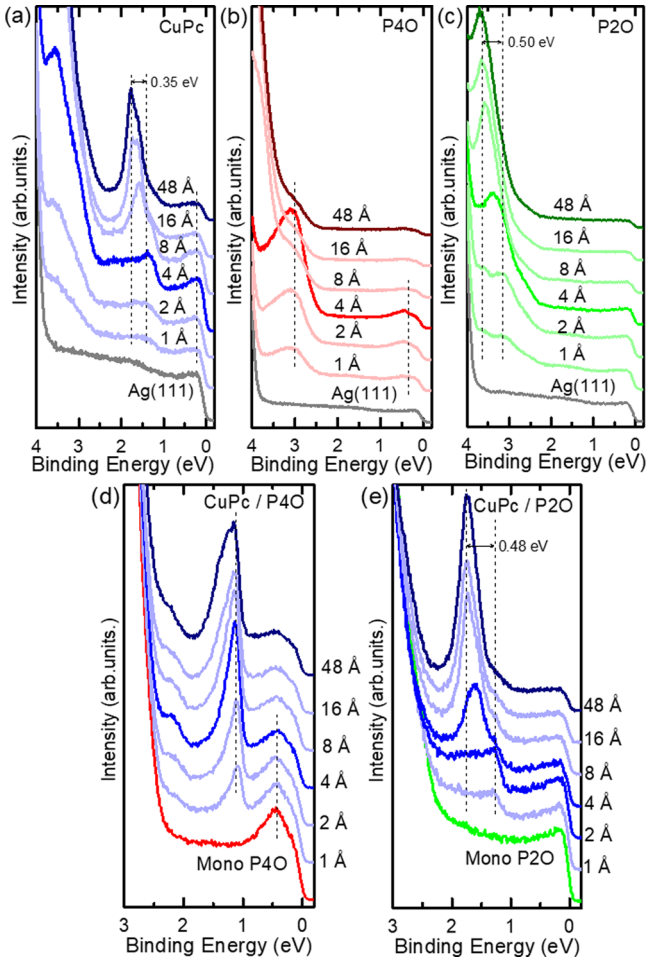

Figure 6. (a–c) UP spectra for stepwise deposited COMs on Ag(111). Monolayer and multilayer spectra are highlighted by darker lines. (d, e) UP spectra for stepwise deposited CuPc on monolayers of P*x*O/Ag(111) (prepared by thermally desorbing the multilayers). For CuPc on P2O/Ag(111) also, the first CuPc spectrum dominated by multilayer features is highlighted. Vertical lines highlight the position of the HOMO and the F-LUMO. Survey spectra (up to 14 eV BE) of these interfaces can be found in Figure S8.

Ag(111). The situation is strikingly different for CuPc deposited on a P2O monolayer on Ag(111). Here, CuPc monolayer features become visible, which can be explained with CuPc reaching the metal surface and forming a charge-transfer complex with Ag(111).

Vacuum-Level Shift ΔVL Determined by Ultraviolet Photoelectron Spectroscopy. The vacuum level (VL) position with increasing film coverage (Figure 7) provides further insight into the interfacial interaction strength at the organic/metal and organic/organic interface and the morphology of the thin film.[69−71] In all cases, the work function of clean Ag(111) is 4.60 eV. Upon initial deposition of CuPc or P2O, the vacuum level shows a steep decrease, which almost saturates at a nominal coverage of 4 Å and stays essentially constant for higher coverages. This behavior confirms flat-lying molecules in the monolayer and predominat multilayer growth for thicknesses larger than 4 Å. For P2O, ΔVL is 0.60 eV and can be mainly ascribed to the push-back effect,[72,73] with ΔVL increasing for decreasing adsorption distance.[74,75] For CuPc, ΔVL is smaller (0.41 eV), as the push-back induced decrease of the VL is partly counteracted by a charge transfer from the

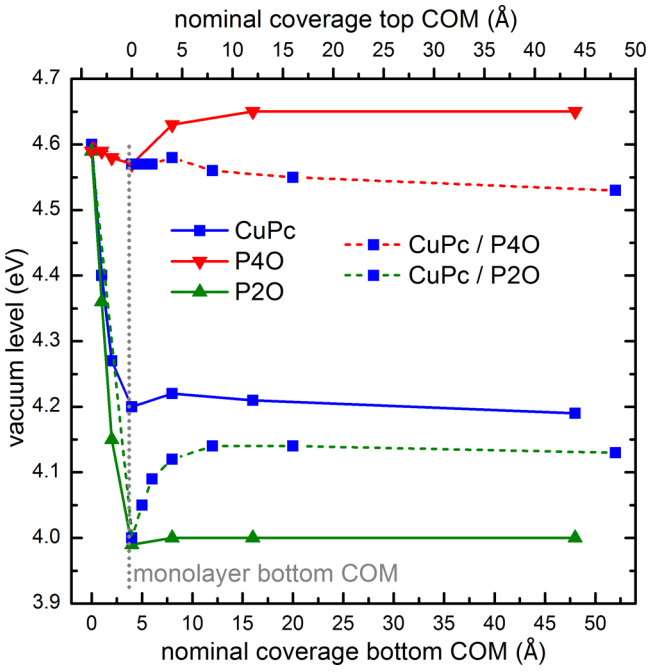

Figure 7. Coverage-dependent evolution of vacuum levels wrt the Fermi level for all investigated thin films on Ag(111). "Bottom" and "top" COM denote the deposition sequence and not the actual arrangement of the thin films. The solid lines correspond to the homomolecular systems and are referred to the bottom abscissa. The dashed lines describe the heteromolecular systems created upon the deposition of increasing coverages of CuPc (referred to the top abscissa) on a full monolayer of P*x*O.

substrate.[59,76] For P4O on the clean substrate, ΔVL is negligible for coverages less than 4 Å, reflecting the larger net electron transfer from the substrate compared with CuPc. For coverages beyond a monolayer, the VL increases slightly, which is most likely due to a band-bending-like effect[67,68] in multilayers.

Deposition of CuPc on P4O/Ag(111) does not result in notable changes of the VL because of the weak coupling at this interface. Deposition of CuPc on P2O/Ag(111), however, increases the VL due to the charge transfer between CuPc and Ag(111). The shift saturates for a nominal CuPc coverage of 8 Å at almost the same value (~4.15 eV) than for CuPc deposited directly on Ag(111). This shows that (i) in the heterostructure, almost the entire metal surface becomes covered by CuPc molecules and (ii) that the energy-level alignment in this case is predominantly determined by the interface dipole upon CuPc monolayer formation.

DISCUSSION

From a device perspective, P4O serves the purpose of lowering the hole injection barrier into multilayers of CuPc on Ag(111) (compare Figure 6a,d), whereas P2O clearly does not decrease the electron-injection barrier (compare Figure 6a,e). The reason for this different behavior becomes evident from STM (Figure 2) and is schematically summarized in Figure 1: CuPc on P4O on Ag(111) forms indeed a bilayer, whereas CuPc deposited on P2O on Ag(111) undergoes molecular exchange and reaches the metal surface.

On the lateral length scale of the STM images, the P2O monolayer is almost closed and rather defect-free (Figure 2e,f). LEED (Figure S2) confirms that order is also preserved at

DOI: 10.1021/acs.jpcc.8b01529
J. Phys. Chem. C 2018, 122, 9480−9490

room temperature (at which thin-film deposition took place). Moreover, we could not observe any changes in the arrangement of P2O−CuPc heterostructures on a time scale of several minutes to several hours after deposition of CuPc. This implies that molecular exchange happens immediately after thin-film preparation and shows that (i) the barrier for replacement is low and (ii) the driving force is high, i.e., as shown by the indicators, CuPc is significantly more favorable on Ag(111) than P2O. Moreover, from STM, it becomes apparent that CuPc and P2O have also no favorable in-plane interaction as they show lateral phase separation after molecular exchange (Figure 2g,h).

Figure 8 shows the five indicators for organic−metal interaction strength. In addition to the indicators for the

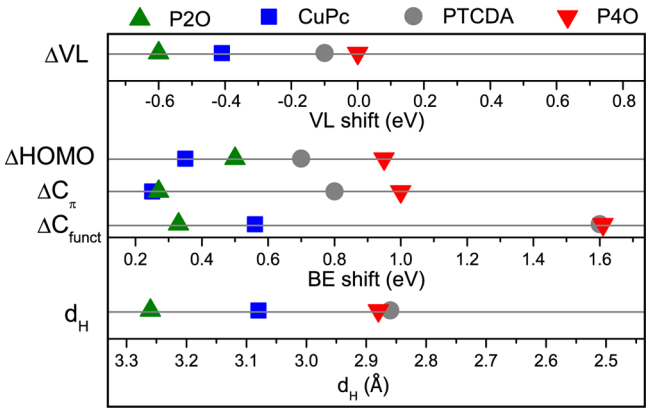

Figure 8. Vacuum-level shift (ΔVL) between clean Ag(111) and a monolayer of the respective COM. Binding-energy shift between monolayer and multilayer of the HOMO-maximum (ΔHOMO) and the C 1s peak of the molecular backbone (ΔC_π) and the functional group (ΔC_{funct}) of the respective COM on Ag(111). Averaged bonding distance (d_H) of the carbon atoms in the molecular core in sub-monolayers on Ag(111). All values of P*x*O as well as ΔVL, ΔHOMO, ΔC_π, and ΔC_{funct} of CuPc are from this work; d_H of CuPc is taken from the literature.[27] For PTCDA, ΔVL, and ΔHOMO are taken from ref 30, d_H from ref 77, and ΔC_π and ΔC_{funct} are estimated from refs 31 and 17.

interaction of CuPc and P*x*O with Ag(111), also PTCDA values taken from literature[17,30,31,77] are included for comparison. Almost all of these values show the same trend in the interaction strength with Ag(111) that increases following the order P2O, CuPc, PTCDA, P4O. This serial order confirms that the rearrangement in the measured bilayers (this work and refs 11, 15) is indeed determined by the coupling of the monolayer with the substrate. As detailed below, all of these five indicators are the result of various (partially competing) effects and their consistency is thus remarkable.

Prior to discussing the UPS- and XPS-derived indicators, it is helpful to distinguish between shifts related to interfacial chemical interactions (and thus to the interaction strength) and shifts having purely electrostatic reasons. The most prominent of the latter one is Fermi-level pinning at the density of (gap) states of the HOMO or LUMO of the adsorbate.[67,68,78] This usually leads to integer charge transfer[35,79,80] and results in a rigid shift of the VL, HOMO (and deeper lying valence levels), and all core levels. From the investigated systems, the LUMO-derived peak in the P2O monolayer (Figure 6c,e) is most likely related to Fermi-level pinning; this is consistent with the onset of the HOMO at around 3 eV below E_F, which is in the range of the optical gap of P2O thin films (2.92 eV).[81] Also, the small VL increase (~0.1 eV) found for P4O on Ag(111) beyond monolayer coverage (Figure 7) points to Fermi-level pinning (at the P4O LUMO). However, the expected shifts in valence and core levels are overcompensated by the strong chemical coupling at this interface. Other electrostatic effects at organic−metal interfaces include the push-back effect[72,73] and the image-charge effect (often called screening),[82,83] which can be held responsible for the rigid shift of HOMO and core-level features for physisorbed P2O on Ag(111). In contrast, chemical interactions usually lead to fractional charge transfer[35,79] often involving donation and backdonation of charges[39,84,85] and thus to nonrigid (chemical) shifts.

Starting the discussion of the indicators with ΔVL, it is noteworthy that for none of the COMs the vacuum level increases upon monolayer formation, which could be naively expected, as in all cases the LUMO becomes (partially) filled for the monolayers on Ag(111). However, ΔVL is the result of many competing effects and without advanced theoretical modeling it is impossible to say whether the expected VL increase is mainly compensated by the push-back effect, backdonation of charges, or distortion-induced intramolecular dipoles. Moreover, obviously a large decrease in the VL as a sign for weak interaction only holds for electron-accepting molecules as for donors, the net electron transfer from the COM to the metal leads to a decrease of the work function beyond push back.[4,86] Consequently, the correct order, with the lowest ΔVL for the strongest interaction, could be merely coincidental and the vacuum level can be considered a weak indicator for interaction strength. A stronger indicator is ΔHOMO, which can distinguish between weak (P2O and CuPc) and strong (PTCDA, P4O) coupling. In the former case, ΔHOMO is dominated by electrostatic effects and in the latter case by molecular relaxations upon charge transfer.[44,87] In general, the fine structure of valence electron features of molecular thin films depends, in addition to interfacial chemical interactions, critically on the thin-film structure. This holds for hole−phonon coupling,[88,89] band dispersion,[90−92] and the photoelectron angular distribution.[93,94] If the molecular thin-film structure in the multilayer differs from that in the monolayer, these effects can lead to an apparent peak maximum shift and can explain the larger shift of P2O compared with CuPc.

Considering the core-level shifts, it is reasonable that the shift of the aromatic carbons' C 1s signal (ΔC_π) is similar to that of the HOMO, as for all four COMs, the HOMO is relatively delocalized over the whole molecule. The widest range (1.6 eV) in BE shifts can be found for the C 1s signals of carbon atoms in functional groups, i.e., C═O or C−N (ΔC_{funct}). This is, on one hand, not surprising, as for hydrocarbon systems, charge transfer is often mediated by functional groups or heteroatoms.[44,95] Then again, the functionality of the heteroatoms is distinctly different for P*x*O, CuPc, and PTCDA and it is not straightforward that also ΔC_{funct} follows the general trend. The same holds for d_H, as averaged vertical bonding distances (and even possible molecular distortions) alone are no clear indication for bonding strength.[40,50,96] For example, it was shown that additional bulky side groups increase the averaged carbon bonding distance of a pyrene derivative on Ag(111) without notable changes in the interaction strength, as measured by UPS and XPS.[40] Moreover, it is only useful to compare bonding distance of different COMs on the same surface.

DOI: 10.1021/acs.jpcc.8b01529
J. Phys. Chem. C 2018, 122, 9480−9490

Overall, the core-level shifts (ΔC_π and ΔC_{funct}) are the most reliable indicators for organic−metal coupling strength. They have furthermore the advantage that, in contrast to d_H, no advanced synchrotron-based measurements are necessary to access them. This applies likewise for valence electron spectra. However, the complex relation of thin-film structure and electronic structure even for weakly interacting systems does not allow to precisely estimate the coupling strength based on single parameters (ΔVL or ΔHOMO). For the considered systems, the indicators predict the sequential arrangement in heterostructures correctly. We note that also other factors such as the particular molecular weight or shape ("bulkiness") may also condition the molecular exchange,[97,98] besides the organic−metal interaction strength.

CONCLUSIONS

The arrangement in organic heterostructures is of utmost importance for controlling the performance of organic (opto)electronic devices, and predicting possible molecular exchange for a COM-pair on an inorganic substrate is indispensable for rational device design. However, even for model systems, molecular exchange mechanisms are not fully understood. The pentacene oxo-derivatives P2O and P4O help to overcome this issue, as a subtle change in chemical structure, adding two more oxygen atoms, has a paramount effect on interfacial coupling with Ag(111): P2O is physisorbed whereas P4O is clearly chemisorbed, as evidenced by UPS, XPS, and XSW. Therefore, subsequently deposited CuPc diffuses through P2O monolayers but forms bilayer structures on P4O, as evidenced by STM. We could show that organic−inorganic coupling is crucial for molecular exchange and that organic−organic coupling plays a minor role in this context. Moreover, we developed simple indicators, i.e., binding-energy shifts in UPS or XPS, which can reliably predict molecular exchange of a COM-pair on a specific substrate. Moreover, quantification of coupling strength based on relatively routine photoemission experiments would be an important step to come closer to a simple and reliable prediction of energy-level alignment at organic−metal interfaces.

ASSOCIATED CONTENT

Supporting Information

The Supporting Information is available free of charge on the ACS Publications website at DOI: 10.1021/acs.jpcc.8b01529.

Temperature-programmed XPS during desorption of the P*x*O multilayers, LEED measurements of P*x*O monolayers at room temperature, additional STM images, N 1s core-level measurements corresponding to CuPc for the systems studied, XSW results and additional UPS measurements (PDF)

AUTHOR INFORMATION

Corresponding Authors

*E-mail: chilf@suda.edu.cn (L.C.).
*E-mail: duhm@suda.edu.cn (S.D.).
*E-mail: frank.schreiber@uni-tuebingen.de (F.S.).

ORCID

Pardeep Kumar Thakur: 0000-0002-9599-0531
Steffen Duhm: 0000-0002-5099-5929

Author Contributions

⊥Q.W. and A.F.-C. contributed equally.

Notes

The authors declare no competing financial interest.

ACKNOWLEDGMENTS

We acknowledge Diamond Light Source for access to beamline I09 that contributed to the results presented here. Financial support from the Major State Basic Research Development Program of China (973 Program, No. 2014CB932600), the National Key R&D Program of China (No. 2017YFA0205002), the Soochow University-Western University Center for Synchrotron Radiation Research, the 111 Project of the Chinese State Administration of Foreign Experts Affairs, the Collaborative Innovation Center of Suzhou Nano Science & Technology (NANO-CIC), and the DFG is gratefully acknowledged. Q.W. also thanks the China Scholarship Council for financial support.

REFERENCES

(1) Street, R. A. Electronic Structure and Properties of Organic Bulk-Heterojunction Interfaces. *Adv. Mater.* **2016**, *28*, 3814−3830.
(2) Yang, J.; Yan, D.; Jones, T. S. Molecular Template Growth and Its Applications in Organic Electronics and Optoelectronics. *Chem. Rev.* **2015**, *115*, 5570−5603.
(3) Zhang, X.; Shao, Z.; Zhang, X.; He, Y.; Jie, J. Surface Charge Transfer Doping of Low-Dimensional Nanostructures toward High-Performance Nanodevices. *Adv. Mater.* **2016**, *28*, 10409−10442.
(4) Akaike, K.; Nardi, M. V.; Oehzelt, M.; Frisch, J.; Opitz, A.; Christodoulou, C.; Ligorio, G.; Beyer, P.; Timpel, M.; Pis, I.; Bondino, F.; Moudgil, K.; Barlow, S.; Marder, S. R.; Koch, N. Effective Work Function Reduction of Practical Electrodes Using an Organometallic Dimer. *Adv. Funct. Mater.* **2016**, *26*, 2493−2502.
(5) Amsalem, P.; Wilke, A.; Frisch, J.; Niederhausen, J.; Vollmer, A.; Rieger, R.; Müllen, K.; Rabe, J. P.; Koch, N. Interlayer molecular diffusion and thermodynamic equilibrium in organic heterostructures on a metal electrode. *J. Appl. Phys.* **2011**, *110*, No. 113709.
(6) Zhang, L.; Zu, F. S.; Deng, Y. L.; Igbari, F.; Wang, Z. K.; Liao, L. S. Origin of Enhanced Hole Injection in Organic Light-Emitting Diodes with an Electron-Acceptor Doping Layer: p-Type Doping or Interfacial Diffusion? *ACS Appl. Mater. Interfaces* **2015**, *7*, 11965−11971.
(7) Li, J.; Rochester, C. W.; Jacobs, I. E.; Friedrich, S.; Stroeve, P.; Riede, M.; Moule, A. J. Measurement of Small Molecular Dopant F4TCNQ and C60F36 Diffusion in Organic Bilayer Architectures. *ACS Appl. Mater. Interfaces* **2015**, *7*, 28420−28428.
(8) Duhm, S.; Salzmann, I.; Bröker, B.; Glowatzki, H.; Johnson, R. L.; Koch, N. Interdiffusion of molecular acceptors through organic layers to metal substrates mimics doping-related energy level shifts. *Appl. Phys. Lett.* **2009**, *95*, No. 093305.
(9) Sun, L.; Liu, C.; Queteschiner, D.; Weidlinger, G.; Zeppenfeld, P. Layer inversion in organic heterostructures. *Phys. Chem. Chem. Phys.* **2011**, *13*, 13382−13386.
(10) Gallego, J. M.; Ecija, D.; Martin, N.; Otero, R.; Miranda, R. An STM study of molecular exchange processes in organic thin film growth. *Chem. Commun.* **2014**, *50*, 9954−9957.
(11) Stadtmüller, B.; Gruenewald, M.; Peuker, J.; Forker, R.; Fritz, T.; Kumpf, C. Molecular Exchange in a Heteromolecular PTCDA/CuPc Bilayer Film on Ag(111). *J. Phys. Chem. C* **2014**, *118*, 28592−28602.
(12) Stadtmüller, B.; Sueyoshi, T.; Kichin, G.; Kröger, I.; Soubatch, S.; Temirov, R.; Tautz, F. S.; Kumpf, C. Commensurate Registry and Chemisorption at a Hetero-organic Interface. *Phys. Rev. Lett.* **2012**, *108*, No. 106103.
(13) Sellam, F.; Schmitz-Hübsch, T.; Toerker, M.; Mannsfeld, S.; Proehl, H.; Fritz, T.; Leo, K.; Simpson, C.; Müllen, K. LEED and STM investigations of organic-organic heterostructures grown by molecular beam epitaxy. *Surf. Sci.* **2001**, *478*, 113−121.
(14) Gruenewald, M.; Sauer, C.; Peuker, J.; Meissner, M.; Sojka, F.; Schöll, A.; Reinert, F.; Forker, R.; Fritz, T. Commensurism at

DOI: 10.1021/acs.jpcc.8b01529
J. Phys. Chem. C 2018, 122, 9480−9490

electronically weakly interacting phthalocyanine/PTCDA heterointerfaces. *Phys. Rev. B* **2015**, *91*, No. 155432.
(15) Stadtmüller, B.; Willenbockel, M.; Schröder, S.; Kleimann, C.; Reinisch, E. M.; Ules, T.; Soubatch, S.; Ramsey, M. G.; Tautz, F. S.; Kumpf, C. Modification of the PTCDA-Ag bond by forming a heteromolecular bilayer film. *Phys. Rev. B* **2015**, *91*, No. 155433.
(16) Kleimann, C.; Stadtmüller, B.; Schröder, S.; Kumpf, C. Electrostatic Interaction and Commensurate Registry at the Heteromolecular F16CuPc-CuPc Interface. *J. Phys. Chem. C* **2014**, *118*, 1652−1660.
(17) Häming, M.; Greif, M.; Sauer, C.; Schöll, A.; Reinert, F. Electronic structure of ultrathin heteromolecular organic-metal interfaces: SnPc/PTCDA/Ag(111) and SnPc/Ag(111). *Phys. Rev. B* **2010**, *82*, No. 235432.
(18) Borghetti, P.; de Oteyza, D. G.; Rogero, C.; Goiri, E.; Verdini, A.; Cossaro, A.; Floreano, L.; Ortega, J. E. Molecular-Level Realignment in Donor-Acceptor Bilayer Blends on Metals. *J. Phys. Chem. C* **2016**, *120*, 5997−6005.
(19) Goiri, E.; Borghetti, P.; El-Sayed, A.; Ortega, J. E.; de Oteyza, D. G. Multi-Component Organic Layers on Metal Substrates. *Adv. Mater.* **2016**, *28*, 1340−1368.
(20) Bouju, X.; Mattioli, C.; Franc, G.; Pujol, A.; Gourdon, A. Bicomponent Supramolecular Architectures at the Vacuum-Solid Interface. *Chem. Rev.* **2017**, *117*, 1407−1444.
(21) El-Sayed, A.; Borghetti, P.; Goiri, E.; Rogero, C.; Floreano, L.; Lovat, G.; Mowbray, D. J.; Cabellos, J. L.; Wakayama, Y.; Rubio, A.; Ortega, J. E.; de Oteyza, D. G. Understanding Energy-Level Alignment in Donor-Acceptor/Metal Interfaces from Core-Level Shifts. *ACS Nano* **2013**, *7*, 6914−6920.
(22) Wakayama, Y. On-surface molecular nanoarchitectonics: From self-assembly to directed assembly. *Jpn. J. Appl. Phys.* **2016**, *55*, No. 1102AA.
(23) Henneke, C.; Felter, J.; Schwarz, D.; Tautz, F. S.; Kumpf, C. Controlling the growth of multiple ordered heteromolecular phases by utilizing intermolecular repulsion. *Nat. Mater.* **2017**, *16*, 628−633.
(24) Thussing, S.; Jakob, P. Thermal Stability and Interlayer Exchange Processes in Heterolayers of CuPc and PTCDA on Ag(111). *J. Phys. Chem. C* **2017**, *121*, 13680−13691.
(25) Egger, D. A.; Ruiz, V. G.; Saidi, W. A.; Bucko, T.; Tkatchenko, A.; Zojer, E. Understanding Structure and Bonding of Multilayered Metal-Organic Nanostructures. *J. Phys. Chem. C* **2013**, *117*, 3055−3061.
(26) Thussing, S.; Jakob, P. Structural and Vibrational Properties of CuPc/Ag(111) Ultrathin Films. *J. Phys. Chem. C* **2016**, *120*, 9904−9913.
(27) Kröger, I.; Stadtmüller, B.; Stadler, C.; Ziroff, J.; Kochler, M.; Stahl, A.; Pollinger, F.; Lee, T.-L.; Zegenhagen, J.; Reinert, F.; Kumpf, C. Submonolayer growth of copper-phthalocyanine on Ag(111). *New J. Phys.* **2010**, *12*, No. 083038.
(28) Hauschild, A.; Karki, K.; Cowie, B. C. C.; Rohlfing, M.; Tautz, F. S.; Sokolowski, M. Molecular Distortions and Chemical Bonding of a Large π-Conjugated Molecule on a Metal Surface. *Phys. Rev. Lett.* **2005**, *94*, No. 036106.
(29) Kilian, L.; Hauschild, A.; Temirov, R.; Soubatch, S.; Schöll, A.; Bendounan, A.; Reinert, F.; Lee, T.-L.; Tautz, F. S.; Sokolowski, M.; Umbach, E. Role of Intermolecular Interactions on the Electronic and Geometric Structure of a Large pi-Conjugated Molecule Adsorbed on a Metal Surface. *Phys. Rev. Lett.* **2008**, *100*, No. 136103.
(30) Duhm, S.; Gerlach, A.; Salzmann, I.; Bröker, B.; Johnson, R. L.; Schreiber, F.; Koch, N. PTCDA on Au(111), Ag(111) and Cu(111): Correlation of interface charge transfer to bonding distance. *Org. Electron.* **2008**, *9*, 111−118.
(31) Zou, Y.; Kilian, L.; Schöll, A.; Schmidt, T.; Fink, R.; Umbach, E. Chemical bonding of PTCDA on Ag surfaces and the formation of interface states. *Surf. Sci.* **2006**, *600*, 1240−1251.
(32) Liu, W.; Filimonov, S. N.; Carrasco, J.; Tkatchenko, A. Molecular switches from benzene derivatives adsorbed on metal surfaces. *Nat. Commun.* **2013**, *4*, No. 2569.
(33) Jakobs, S.; Narayan, A.; Stadtmüller, B.; Droghetti, A.; Rungger, I.; Hor, Y. S.; Klyatskaya, S.; Jungkenn, D.; Stöckl, J.; Laux, M.; et al. Controlling the Spin Texture of Topological Insulators by Rational Design of Organic Molecules. *Nano Lett.* **2015**, *15*, 6022−6029.
(34) Maurer, R. J.; Ruiz, V. G.; Camarillo-Cisneros, J.; Liu, W.; Ferri, N.; Reuter, K.; Tkatchenko, A. Adsorption structures and energetics of molecules on metal surfaces: Bridging experiment and theory. *Prog. Surf. Sci.* **2016**, *91*, 72−100.
(35) Hollerer, M.; Lüftner, D.; Hurdax, P.; Ules, T.; Soubatch, S.; Tautz, F. S.; Koller, G.; Puschnig, P.; Sterrer, M.; Ramsey, M. G. Charge Transfer and Orbital Level Alignment at Inorganic/Organic Interfaces: The Role of Dielectric Interlayers. *ACS Nano* **2017**, *11*, 6252−6260.
(36) Obersteiner, V.; Scherbela, M.; Hörmann, L.; Wegner, D.; Hofmann, O. T. Structure Prediction for Surface-Induced Phases of Organic Monolayers: Overcoming the Combinatorial Bottleneck. *Nano Lett.* **2017**, *17*, 4453−4460.
(37) Woodruff, D. P. Surface structure determination using x-ray standing waves. *Rep. Prog. Phys.* **2005**, *68*, 743−798.
(38) Zegenhagen, J. Surface Structure Analysis with X-Ray Standing Waves. In *Springer Series in Surface Sciences*; Bracco, G., Holst, B., Eds.; Springer: Berlin, 2013; Vol. *51*, pp 249−275.
(39) Zamborlini, G.; Lüftner, D.; Feng, Z.; Kollmann, B.; Puschnig, P.; Dri, C.; Panighel, M.; Di Santo, G.; Goldoni, A.; Comelli, G.; Jugovac, M.; Feyer, V.; Schneidery, C. M. Multi-orbital charge transfer at highly oriented organic/metal interfaces. *Nat. Commun.* **2017**, *8*, No. 335.
(40) Hofmann, O. T.; Glowatzki, H.; Bürker, C.; Rangger, G. M.; Bröker, B.; Niederhausen, J.; Hosokai, T.; Salzmann, I.; Blum, R.-P.; Rieger, R.; et al. Orientation-Dependent Work-Function Modification Using Substituted Pyrene-Based Acceptors. *J. Phys. Chem. C* **2017**, *121*, 24657−24668.
(41) Riss, A.; Paz, A. P.; Wickenburg, S.; Tsai, H.-Z.; De Oteyza, D. G.; Bradley, A. J.; Ugeda, M. M.; Gorman, P.; Jung, H. S.; Crommie, M. F.; Rubio, A.; Fischer, F. R. Imaging single-molecule reaction intermediates stabilized by surface dissipation and entropy. *Nat. Chem.* **2016**, *8*, 678−683.
(42) Jiang, L.; Papageorgiou, A. C.; Oh, S. C.; Saglam, O.; Reichert, J.; Duncan, D. A.; Zhang, Y.-Q.; Klappenberger, F.; Guo, Y.; Allegretti, F.; More, S.; Bhosale, R.; Mateo-Alonso, A.; Barth, J. V. Synthesis of Pyrene-Fused Pyrazaacenes on Metal Surfaces: Toward One-Dimensional Conjugated Nanostructures. *ACS Nano* **2016**, *10*, 1033−1041.
(43) Ugolotti, A.; Harivyasi, S. S.; Baby, A.; Dominguez, M.; Pinardi, A. L.; Lopez, M. F.; Martin-Gago, J. A.; Fratesi, G.; Floreano, L.; Brivio, G. P. Chemisorption of Pentacene on Pt(111) with a Little Molecular Distortion. *J. Phys. Chem. C* **2017**, *121*, 22797−22805.
(44) Heimel, G.; Duhm, S.; Salzmann, I.; Gerlach, A.; Strozecka, A.; Niederhausen, J.; Bürker, C.; Hosokai, T.; Fernandez-Torrente, I.; Schulze, G.; et al. Charged and metallic molecular monolayers through surface-induced aromatic stabilization. *Nat. Chem.* **2013**, *5*, 187−194.
(45) Yang, A.; Franco-Cañellas, A.; Sato, M.; Wang, B.; Wang, R.-B.; Koike, H.; Salzmann, I.; Thakur, P. K.; Lee, T.-L.; Liu, L.; Kera, S.; et al. Nitrogen substitution impacts organic-metal interface energetics. *Phys. Rev. B* **2016**, *94*, No. 155426.
(46) Lu, M.-C.; Wang, R.-B.; Yang, A.; Duhm, S. Pentacene on Au(111), Ag(111) and Cu(111): From physisorption to chemisorption. *J. Phys.: Condens. Matter* **2016**, *28*, No. 094005.
(47) Bürker, C.; Franco-Cañellas, A.; Broch, K.; Lee, T.-L.; Gerlach, A.; Schreiber, F. Self-Metalation of 2H-Tetraphenylporphyrin on Cu(111) Studied with XSW: Influence of the Central Metal Atom on the Adsorption Distance. *J. Phys. Chem. C* **2014**, *118*, 13659−13666.
(48) Manandhar, K.; Ellis, T.; Park, K.; Cai, T.; Song, Z.; Hrbek, J. A scanning tunneling microscopy study on the effect of post-deposition annealing of copper phthalocyanine thin films. *Surf. Sci.* **2007**, *601*, 3623−3631.
(49) Ruocco, A.; Evangelista, F.; Gotter, R.; Attili, A.; Stefani, G. Evidence of Charge Transfer at the Cu-phthalocyanine/Al(100) Interface. *J. Phys. Chem. C* **2008**, *112*, 2016−2025.

DOI: 10.1021/acs.jpcc.8b01529
J. Phys. Chem. C 2018, 122, 9480−9490

(50) Franco-Cañellas, A.; Wang, Q.; Broch, K.; Duncan, D. A.; Thakur, P. K.; Liu, L.; Kera, S.; Gerlach, A.; Duhm, S.; Schreiber, F. Metal-organic interface functionalization via acceptor end groups: PTCDI on coinage metals. *Phys. Rev. Mater.* **2017**, *1*, No. 013001.
(51) Häming, M.; Schöll, A.; Umbach, E.; Reinert, F. Adsorbate-substrate charge transfer and electron-hole correlation at adsorbate/metal interfaces. *Phys. Rev. B* **2012**, *85*, No. 235132.
(52) Borghetti, P.; El-Sayed, A.; Goiri, E.; Rogero, C.; Lobo-Checa, J.; Floreano, L.; Ortega, J. E.; de Oteyza, D. G. Spectroscopic Fingerprints of Work-Function-Controlled Phthalocyanine Charging on Metal Surfaces. *ACS Nano* **2014**, *8*, 12786−12795.
(53) Evangelista, F.; Carravetta, V.; Stefani, G.; Jansik, B.; Alagia, M.; Stranges, S.; Ruocco, A. Electronic structure of copper phthalocyanine: An experimental and theoretical study of occupied and unoccupied levels. *J. Chem. Phys.* **2007**, *126*, No. 124709.
(54) Sinha, S.; Mukherjee, M. Study of metal specific interaction, F-LUMO and VL shift to understand interface of CuPc thin films and noble metal surfaces. *Appl. Surf. Sci.* **2015**, *353*, 540−547.
(55) Peisert, H.; Knupfer, M.; Schwieger, T.; Auerhammer, J. M.; Golden, M. S.; Fink, J. Full characterization of the interface between the organic semiconductor copper phthalocyanine and gold. *J. Appl. Phys.* **2002**, *91*, 4872−4878.
(56) Koch, N. Energy levels at interfaces between metals and conjugated organic molecules. *J. Phys.: Condens. Matter* **2008**, *20*, No. 184008.
(57) Otero, R.; Vázquez de Parga, A.; Gallego, J. Electronic, structural and chemical effects of charge-transfer at organic/inorganic interfaces. *Surf. Sci. Rep.* **2017**, *72*, 105−145.
(58) Stadtmüller, B.; Schröder, S.; Kumpf, C. Heteromolecular metal-organic interfaces: Electronic and structural fingerprints of chemical bonding. *J. Electron Spectrosc. Relat. Phenom.* **2015**, *204*, 80−91.
(59) Duhm, S.; Bürker, C.; Hosokai, T.; Gerlach, A. Vertical Bonding Distances Impact Organic-Metal Interface Energetics. In *Springer Series in Materials Science*; Ishii, H., Kudo, K., Nakayama, T., Ueno, N., Eds.; Springer: Japan, 2015; Vol. *209*, pp 89−107.
(60) Kröger, I.; Stadtmüller, B.; Kleimann, C.; Rajput, P.; Kumpf, C. Normal-incidence x-ray standing-wave study of copper phthalocyanine submonolayers on Cu(111) and Au(111). *Phys. Rev. B* **2011**, *83*, No. 195414.
(61) van Straaten, G.; Franke, M.; Bocquet, F. C.; Tautz, F. S.; Kumpf, C. Non-dipolar effects in photoelectron-based normal incidence x-ray standing wave experiments. *J. Electron Spectrosc. Relat. Phenom.* **2018**, *222*, 106−116.
(62) Blowey, P. J.; Rochford, L. A.; Duncan, D. A.; Warr, D. A.; Lee, T.-L.; Woodruff, D. P.; Costantini, G. Probing the interplay between geometric and electronic structure in a two-dimensional K-TCNQ charge transfer network. *Faraday Discuss.* **2017**, *204*, 97−110.
(63) Stadtmüller, B.; Schröder, S.; Bocquet, F. C.; Henneke, C.; Kleimann, C.; Soubatch, S.; Willenbockel, M.; Detlefs, B.; Zegenhagen, J.; Lee, T.-L.; Tautz, F. S.; Kumpf, C. Adsorption height alignment at heteromolecular hybrid interfaces. *Phys. Rev. B* **2014**, *89*, No. 161407.
(64) Goiri, E.; Matena, M.; El-Sayed, A.; Lobo-Checa, J.; Borghetti, P.; Rogero, C.; Detlefs, B.; Duvernay, J.; Ortega, J. E.; de Oteyza, D. G. Self-Assembly of Bicomponent Molecular Monolayers: Adsorption Height Changes and Their Consequences. *Phys. Rev. Lett.* **2014**, *112*, No. 117602.
(65) Stadtmüller, B.; Lüftner, D.; Willenbockel, M.; Reinisch, E. M.; Sueyoshi, T.; Koller, G.; Soubatch, S.; Ramsey, M. G.; Puschnig, P.; Tautz, F. S.; Kumpf, C. Unexpected interplay of bonding height and energy level alignment at heteromolecular hybrid interfaces. *Nat. Commun.* **2014**, *5*, No. 3685.
(66) Ziroff, J.; Hame, S.; Kochler, M.; Bendounan, A.; Schöll, A.; Reinert, F. Low-energy scale excitations in the spectral function of organic monolayer systems. *Phys. Rev. B* **2012**, *85*, No. 161404.
(67) Yang, J.-P.; Bussolotti, F.; Kera, S.; Ueno, N. Origin and role of gap states in organic semiconductor studied by UPS: as the nature of organic molecular crystals. *J. Phys. D: Appl. Phys.* **2017**, *50*, No. 423002.
(68) Oehzelt, M.; Koch, N.; Heimel, G. Organic semiconductor density of states controls the energy level alignment at electrode interfaces. *Nat. Commun.* **2014**, *5*, No. 4174.
(69) Schultz, T.; Lenz, T.; Kotadiya, N.; Heimel, G.; Glasser, G.; Berger, R.; Blom, P. W. M.; Amsalem, P.; de Leeuw, D. M.; Koch, N. Reliable Work Function Determination of Multicomponent Surfaces and Interfaces: The Role of Electrostatic Potentials in Ultraviolet Photoelectron Spectroscopy. *Adv. Mater. Interfaces* **2017**, *4*, No. 1700324.
(70) Cahen, D.; Kahn, A. Electron Energetics at Surfaces and Interfaces: Concepts and Experiments. *Adv. Mater.* **2003**, *15*, 271−277.
(71) Wang, Q.; Xin, Q.; Wang, R.-B.; Oehzelt, M.; Ueno, N.; Kera, S.; Duhm, S. Picene thin films on metal surfaces: Impact of molecular shape on interfacial coupling. *Phys. Status Solidi RRL* **2017**, *11*, No. 1700012.
(72) Koch, N. Organic Electronic Devices and Their Functional Interfaces. *ChemPhysChem* **2007**, *8*, 1438−1455.
(73) Bagus, P. S.; Staemmler, V.; Wöll, C. Exchange-like Effects for Closed-Shell Adsorbates: Interface Dipole and Work Function. *Phys. Rev. Lett.* **2002**, *89*, No. 096104.
(74) Toyoda, K.; Hamada, I.; Lee, K.; Yanagisawa, S.; Morikawa, Y. Density functional theoretical study of pentacene/noble metal interfaces with van der Waals corrections: Vacuum level shifts and electronic structures. *J. Chem. Phys.* **2010**, *132*, No. 134703.
(75) Ferri, N.; Ambrosetti, A.; Tkatchenko, A. Electronic charge rearrangement at metal/organic interfaces induced by weak van der Waals interactions. *Phys. Rev. Mater.* **2017**, *1*, No. 026003.
(76) Rangger, G. M.; Hofmann, O. T.; Romaner, L.; Heimel, G.; Bröker, B.; Blum, R.-P.; Johnson, R. L.; Koch, N.; Zojer, E. F4TCNQ on Cu, Ag, and Au as prototypical example for a strong organic acceptor on coinage metals. *Phys. Rev. B* **2009**, *79*, No. 165306.
(77) Gerlach, A.; Sellner, S.; Schreiber, F.; Koch, N.; Zegenhagen, J. Substrate-dependent bonding distances of PTCDA: A comparative x-ray standing-wave study on Cu(111) and Ag(111). *Phys. Rev. B* **2007**, *75*, No. 045401.
(78) Bussolotti, F.; Kera, S.; Kudo, K.; Kahn, A.; Ueno, N. Gap states in Pentacene Thin Film Induced by Inert Gas Exposure. *Phys. Rev. Lett.* **2013**, *110*, No. 267602.
(79) Hofmann, O. T.; Rinke, P.; Scheffler, M.; Heimel, G. Integer versus Fractional Charge Transfer at Metal(/Insulator)/Organic Interfaces: Cu(/NaCl)/TCNE. *ACS Nano* **2015**, *9*, 5391−5404.
(80) Winkler, S.; Amsalem, P.; Frisch, J.; Oehzelt, M.; Heimel, G.; Koch, N. Probing the energy levels in hole-doped molecular semiconductors. *Mater. Horiz.* **2015**, *2*, 427−433.
(81) Salzmann, I.; Opitz, R.; Rogaschewski, S.; Rabe, J. P.; Koch, N.; Nickel, B. Phase separation in vacuum co-deposited pentacene/6,13-pentacenequinone thin films. *Phys. Rev. B* **2007**, *75*, No. 174108.
(82) Hill, I. G.; Mäkinen, A. J.; Kafafi, Z. H. Initial stages of metal/organic semiconductor interface formation. *J. Appl. Phys.* **2000**, *88*, 889−895.
(83) Liu, Z.-F.; Egger, D. A.; Refaely-Abramson, S.; Kronik, L.; Neaton, J. B. Energy level alignment at molecule-metal interfaces from an optimally tuned range-separated hybrid functional. *J. Chem. Phys.* **2017**, *146*, No. 092326.
(84) Romaner, L.; Heimel, G.; Brédas, J.-L.; Gerlach, A.; Schreiber, F.; Johnson, R. L.; Zegenhagen, J.; Duhm, S.; Koch, N.; Zojer, E. Impact of Bidirectional Charge Transfer and Molecular Distortions on the Electronic Structure of a Metal-Organic Interface. *Phys. Rev. Lett.* **2007**, *99*, No. 256801.
(85) Tseng, T.-C.; Urban, C.; Wang, Y.; Otero, R.; Tait, S. L.; Alcami, M.; Ecija, D.; Trelka, M.; Gallego, J. M.; Lin, N.; et al. Charge-transfer-induced structural rearrangements at both sides of organic/metal interfaces. *Nat. Chem.* **2010**, *2*, 374−379.
(86) Bröker, B.; Blum, R.-P.; Frisch, J.; Vollmer, A.; Hofmann, O. T.; Rieger, R.; Müllen, K.; Rabe, J. P.; Zojer, E.; Koch, N. Gold work function reduction by 2.2 eV with an air-stable molecular donor layer. *Appl. Phys. Lett.* **2008**, *93*, No. 243303.
(87) Brédas, J.-L.; Beljonne, D.; Coropceanu, V.; Cornil, J. Charge-Transfer and Energy-Transfer Processes in π-Conjugated Oligomers

DOI: 10.1021/acs.jpcc.8b01529
J. Phys. Chem. C 2018, 122, 9480−9490

and Polymers: A Molecular Picture. *Chem. Rev.* **2004**, *104*, 4971−5004.
(88) He, Y.; Bussolotti, F.; Xin, Q.; Yang, J.; Kera, S.; Ueno, N.; Duhm, S. Transient Monolayer Structure of Rubrene on Graphite: Impact on Hole-Phonon Coupling. *J. Phys. Chem. C* **2016**, *120*, 14568−14574.
(89) Kera, S.; Yamane, H.; Ueno, N. First-principles measurements of charge mobility in organic semiconductors: Valence hole-vibration coupling in organic ultrathin films. *Prog. Surf. Sci.* **2009**, *84*, 135−154.
(90) Koller, G.; Berkebile, S.; Oehzelt, M.; Puschnig, P.; Ambrosch-Draxl, C.; Netzer, F. P.; Ramsey, M. G. Intra- and Intermolecular Band Dispersion in an Organic Crystal. *Science* **2007**, *317*, 351−355.
(91) Yamane, H.; Kosugi, N. Substituent-Induced Intermolecular Interaction in Organic Crystals Revealed by Precise Band-Dispersion Measurements. *Phys. Rev. Lett.* **2013**, *111*, No. 086602.
(92) Ueno, N.; Kera, S. Electron spectroscopy of functional organic thin films: Deep insights into valence electronic structure in relation to charge transport property. *Prog. Surf. Sci.* **2008**, *83*, 490−557.
(93) Liu, Y.; Ikeda, D.; Nagamatsu, S.; Nishi, T.; Ueno, N.; Kera, S. Impact of molecular orbital distribution on photoelectron intensity for picene film. *J. Electron Spectrosc. Relat. Phenom.* **2014**, *195*, 287−292.
(94) Puschnig, P.; Berkebile, S.; Fleming, A. J.; Koller, G.; Emtsev, K.; Seyller, T.; Riley, J. D.; Ambrosch-Draxl, C.; Netzer, F. P.; Ramsey, M. G. Reconstruction of Molecular Orbital Densities from Photoemission Data. *Science* **2009**, *326*, 702−706.
(95) Peisert, H.; Uihlein, J.; Petraki, F.; Chasse, T. Charge transfer between transition metal phthalocyanines and metal substrates: The role of the transition metal. *J. Electron Spectrosc. Relat. Phenom.* **2015**, *204*, 49−60.
(96) Willenbockel, M.; Lüftner, D.; Stadtmüller, B.; Koller, G.; Kumpf, C.; Soubatch, S.; Puschnig, P.; Ramsey, M. G.; Tautz, F. S. The interplay between interface structure, energy level alignment and chemical bonding strength at organic-metal interfaces. *Phys. Chem. Chem. Phys.* **2015**, *17*, 1530−1548.
(97) McEwan, J. A.; Clulow, A. J.; Nelson, A.; Wang, R.; Burn, P. L.; Gentle, I. R. Influence of Dopant Concentration and Steric Bulk on Interlayer Diffusion in OLEDs. *Adv. Mater. Interfaces* **2018**, *5*, No. 1700872.
(98) Jacobs, I. E.; Moulé, A. J. Controlling Molecular Doping in Organic Semiconductors. *Adv. Mater.* **2017**, *29*, No. 1703063.

DOI: 10.1021/acs.jpcc.8b01529
J. Phys. Chem. C 2018, 122, 9480−9490